Phase transition from quark-meson coupling hyperonic matter to deconfined quark matter

J. D. Carroll,[*] D. B. Leinweber, and A. G. Williams

Centre for the Subatomic Structure of Matter (CSSM), Department of Physics, University of Adelaide, SA 5005, Australia

A. W. Thomas

Thomas Jefferson National Accelerator Facility, 12000 Jefferson Ave., Newport News, Virginia 23606, USA,
College of William and Mary, Williamsburg, Virginia 23187, USA, and
Centre for the Subatomic Structure of Matter (CSSM), Department of Physics, University of Adelaide, SA 5005, Australia

We investigate the possibility and consequences of phase transitions from an equation of state (EOS) describing nucleons and hyperons interacting via mean fields of σ, ω, and ρ mesons in the recently improved quark-meson coupling (QMC) model to an EOS describing a Fermi gas of quarks in an MIT bag. The transition to a mixed phase of baryons and deconfined quarks, and subsequently to a pure deconfined quark phase, is described using the method of Glendenning. The overall EOS for the three phases is calculated for various scenarios and used to calculate stellar solutions using the Tolman-Oppenheimer-Volkoff equations. The results are compared with recent experimental data, and the validity of each case is discussed with consequences for determining the species content of the interior of neutron stars.

I. INTRODUCTION

The use of hadronic models to describe high-density matter enables us to investigate both the microscopic world of atomic nuclei and the macroscopic world of compact stellar objects, encompassing an enormous range of scales. The results of these investigations provide deep fundamental insight into the way the world around us is constructed.

Experimental data from both extremes of scale aid in constraining such models, from the saturation properties of nuclear matter to the observed properties of neutron stars [1–3]. The literature [4–9] provides a plethora of models for the EOS of hadronic matter, at least some of which have been successfully applied to calculate the properties of finite nuclei. There are also important constraints from data involving heavy-ion collisions [10,11]. Many of these EOSs have also been applied to neutron star features. However, the amount of data available for neutron stars (or compact stellar objects) is very limited, with only a single measurement containing simultaneously both mass and radius bounds [12], and even that has been recently disputed [13].

With such a lack of constraining data, our focus shifts to finding models that better reflect the physics that is expected to be important under the conditions that we are investigating. For example, at the densities considered to be interesting for this investigation (1–10 times nuclear density, $\rho_0 = 0.16$ fm^{-3}), it is possible that either hyperonic matter (in which strangeness carrying baryons become energetically favorable as the Fermi sea fills), quark matter (in which it becomes energetically favorable that the quarks inside the baryons become deconfined), or a mixed phase of these is present, rather than the more traditional treatment of nucleons alone.

We construct a model of high-density matter that is globally charge neutral, color neutral, rotationally symmetric, and in a state that is energetically favorable. For this purpose, we consider hadronic matter modeled by the quark-meson coupling (QMC) model [14,15], which was recently improved through the self-consistent inclusion of color hyperfine interactions [16]. While this improvement had no significant effect on the binding of nucleons, it led to impressive results for finite hypernuclei [17]. We follow the method of Glendenning [18] to produce a mixed phase of hyperonic matter and deconfined quark matter under total mechanical stability, then a pure deconfined quark matter phase with relativistic noninteracting quarks.

We begin with a brief presentation of relativistic mean-field theory in Sec. II to establish a foundation upon which to discuss the general formalism for the QMC model, including new additions, in Sec. III. Deconfined quark matter is discussed in Sec. IV. This is followed by Sec. V providing a summary of the requirements for and method to construct a phase transition from a hadronic phase to a mixed phase and from a mixed phase to a quark phase. Stellar solutions are calculated in Sec. VI, and a summary of our results is presented in Sec. VII, with conclusions in Sec. VIII.

II. RELATIVISTIC MEAN-FIELD THEORY

We introduce the mean-field description of nuclear matter using the classic example of quantum hadrodynamics (QHD) [9,19,20]. Although the quark-meson coupling (QMC) model has a fundamentally different starting point, namely, the self-consistent modification of the structure of a hadron immersed in the nuclear medium [21–23], in practice the equations for nuclear matter involve only a few key differences. We summarize those in the next section. The original formulation of QHD included only nucleons interacting with scalar-isoscalar,

---

[*]jcarroll@physics.adelaide.edu.au

σ, and vector-isoscalar, ω, mesons. This was later expanded to include the vector-isovector, ρ, and subsequently the entire octet of baryons, $B \in \{p, n, \Lambda, \Sigma^+, \Sigma^0, \Sigma^-, \Xi^0, \Xi^-\}$, with global charge neutrality upheld via leptons, $\ell \in \{e^-, \mu^-\}$.

The Lagrangian density for QHD is

$$
\begin{aligned}
\mathcal{L} = \sum_k \bar{\psi}_k [\gamma_\mu (i \partial^\mu - g_{\omega k} \omega^\mu - g_\rho \vec{\tau}_{(k)} \cdot \vec{\rho}^\mu) \\
- (M_k - g_{\sigma k} \sigma)] \psi_k + \frac{1}{2} (\partial_\mu \sigma \partial^\mu \sigma - m_\sigma^2 \sigma^2) \\
- \frac{1}{4} F_{\mu\nu} F^{\mu\nu} - \frac{1}{4} R^a_{\mu\nu} R^{\mu\nu}_a + \frac{1}{2} m_\omega^2 \omega_\mu \omega^\mu \\
+ \frac{1}{2} m_\rho^2 \rho^a_\mu \rho^\mu_a + \bar{\psi}_\ell [\gamma_\mu i \partial^\mu - m_\ell] \psi_\ell + \delta \mathcal{L},
\end{aligned}
\tag{1}
$$

where the index $k \in \{N, \Lambda, \Sigma, \Xi\}$ represents each isospin group of the baryon states, and ψ_k corresponds to the Dirac spinors for these:

$$
\psi_N = \begin{pmatrix} \psi_p \\ \psi_n \end{pmatrix}, \quad \psi_\Lambda = (\psi_\Lambda),
$$

$$
\psi_\Sigma = \begin{pmatrix} \psi_{\Sigma^+} \\ \psi_{\Sigma^0} \\ \psi_{\Sigma^-} \end{pmatrix}, \quad \psi_\Xi = \begin{pmatrix} \psi_{\Xi^0} \\ \psi_{\Xi^-} \end{pmatrix}.
\tag{2}
$$

The vector field tensors are

$$
F^{\mu\nu} = \partial^\mu \omega^\nu - \partial^\nu \omega^\mu,
$$

$$
R^{\mu\nu}_a = \partial^\mu \rho^\nu_a - \partial^\nu \rho^\mu_a - g_\rho \epsilon^{abc} \rho^\mu_b \rho^\nu_c,
\tag{3}
$$

The third components of the isospin matrices are

$$
\tau_{(N)3} = \tau_{(\Xi)3} = \frac{1}{2} \begin{bmatrix} 1 & 0 \\ 0 & -1 \end{bmatrix}, \quad \tau_{(\Lambda)3} = [0],
$$

$$
\tau_{(\Sigma)3} = \begin{bmatrix} 1 & 0 & 0 \\ 0 & 0 & 0 \\ 0 & 0 & -1 \end{bmatrix}.
\tag{4}
$$

ψ_ℓ is a spinor for the lepton states, and $\delta \mathcal{L}$ are renormalization terms. We do not include pions here, as they provide no contribution to the mean field, because the ground state of nuclear matter is parity-even. We have neglected nonlinear meson terms in this description for comparison purposes, though it has been shown that the inclusion of nonlinear scalar meson terms produces a framework consistent with the QMC model without the added hyperfine interaction [24]. The values of the baryon and meson masses in vacuum are summarized in Table I.

Assuming that the baryon density is sufficiently large, we use a mean-field approximation (MFA) with physical parameters (breaking charge symmetry) in which the meson fields are replaced by their classical vacuum expectation values. With this condition, the renormalization terms can be neglected.

By enforcing rotational symmetry and working in the frame where the matter as a whole is at rest, we set all of the three-vector components of the vector meson fields to zero, leaving only the temporal components. Furthermore, by enforcing isospin symmetry, we remove all charged meson states. Consequently, because the mean fields are constant, all meson derivative terms vanish, and thus so do the vector field tensors. The only nonzero components of the vector meson mean fields are then the time components, $\langle \omega^\mu \rangle = \langle \omega \rangle \delta^{\mu 0}$ and $\langle \rho^\mu \rangle = \langle \rho \rangle \delta^{\mu 0}$. Similarly, only the third component of the ρ meson mean field in isospace is nonzero, corresponding to the uncharged ρ meson.

The couplings of the mesons to the baryons are found via SU(6) flavor symmetry [26]. This produces the following relations for the σ and ω couplings to each isospin group (and hence each baryon B in that isospin group):

$$
\frac{1}{3} g_{\sigma N} = \frac{1}{2} g_{\sigma \Lambda} = \frac{1}{2} g_{\sigma \Sigma} = g_{\sigma \Xi},
$$

$$
\frac{1}{3} g_{\omega N} = \frac{1}{2} g_{\omega \Lambda} = \frac{1}{2} g_{\omega \Sigma} = g_{\omega \Xi}.
\tag{5}
$$

Using the formalism as above with isospin expressed explicitly in the Lagrangian density, the couplings of the ρ meson to the octet baryons are unified; thus by specifying $g_{\sigma N}$, $g_{\omega N}$, and g_ρ, we are therefore able to determine the couplings to the remaining baryons.

By evaluating the equations of motion from the Euler-Lagrange equations

$$
\frac{\partial \mathcal{L}}{\partial \phi_i} - \partial_\mu \frac{\partial \mathcal{L}}{\partial (\partial_\mu \phi_i)} = 0,
\tag{6}
$$

we find the mean-field equations for each of the mesons as well as the baryons. The equations for the meson fields are

$$
\langle \sigma \rangle = \sum_B \frac{g_{\sigma B}}{m_\sigma^2} \langle \bar{\psi}_B \psi_B \rangle,
\tag{7}
$$

$$
\langle \omega \rangle = \sum_B \frac{g_{\omega B}}{m_\omega^2} \langle \bar{\psi}_B \gamma^0 \psi_B \rangle = \sum_B \frac{g_{\omega B}}{m_\omega^2} \langle \psi_B^\dagger \psi_B \rangle,
\tag{8}
$$

$$
\langle \rho \rangle = \sum_k \frac{g_\rho}{m_\rho^2} \langle \bar{\psi}_k \gamma^0 \tau_{(k)3} \psi_k \rangle
$$

$$
= \sum_k \frac{g_\rho}{m_\rho^2} \langle \psi_k^\dagger \tau_{(k)3} \psi_k \rangle = \sum_B \frac{g_\rho}{m_\rho^2} \langle \psi_B^\dagger I_{3B} \psi_B \rangle,
\tag{9}
$$

where the sum over B corresponds to the sum over the octet baryon states, and the sum over k corresponds to the sum over isospin groups. I_{3B} is the third component of isospin of baryon B, as found in the diagonal elements of $\tau_{(k)3}$. $\langle \omega \rangle$, $\langle \rho \rangle$,

TABLE I. Vacuum (physical) baryon and meson masses (in MeV) as used here [25].

M_p	M_n	M_Λ	M_{Σ^-}	M_{Σ^0}	M_{Σ^+}	M_{Ξ^-}	M_{Ξ^0}
938.27	939.57	1115.68	1197.45	1192.64	1189.37	1321.31	1314.83

m_σ	m_ω	m_ρ
550.0	782.6	775.8

and $\langle\sigma\rangle$ are proportional to the conserved baryon density, isospin density, and scalar density, respectively, where the scalar density is calculated self-consistently.

The Euler-Lagrange equations also provide a Dirac equation for the baryons

$$\sum_B [i\,\not{\partial} - g_{\omega B}\gamma^0\langle\omega\rangle - g_\rho\gamma^0 I_{3B}\langle\rho\rangle$$
$$- M_B + g_{\sigma B}\langle\sigma\rangle]\psi_B = 0. \tag{10}$$

At this point, we can define the baryon effective mass as

$$M_B^* = M_B - g_{\sigma B}\langle\sigma\rangle, \tag{11}$$

and the baryon chemical potential (also known as the Fermi energy, the energy associated with the Dirac equation) as

$$\mu_B = \epsilon_{F_B} = \sqrt{k_{F_B}^2 + (M_B^*)^2} + g_{\omega B}\langle\omega\rangle + g_\rho I_{3B}\langle\rho\rangle. \tag{12}$$

The chemical potentials for the leptons are found via

$$\mu_\ell = \sqrt{k_{F_\ell}^2 + m_\ell^2}. \tag{13}$$

The energy density $\mathcal{E}$ and pressure P for the EOS can be obtained using the relations for the energy-momentum tensor (where u^μ is the four-velocity)

$$\langle T^{\mu\nu}\rangle = (\mathcal{E} + P)u^\mu u^\nu + Pg^{\mu\nu}, \Rightarrow P = \tfrac{1}{3}\langle T^{ii}\rangle,$$
$$\mathcal{E} = \langle T^{00}\rangle, \tag{14}$$

since $u^i = 0$ and $u_0 u^0 = -1$, where $g^{\mu\nu}$ here is the inverse metric tensor having a negative temporal component, and $T^{\mu\nu}$ is the energy-momentum tensor. In accordance with Noether's theorem, the relation between the energy-momentum tensor and the Lagrangian density is

$$T^{\mu\nu} = -g^{\mu\nu}\mathcal{L} + \partial^\mu\psi\frac{\partial\mathcal{L}}{\partial(\partial_\nu\psi)}, \tag{15}$$

and we find the Hartree-level energy density and pressure for the system as a sum of contributions from baryons B, leptons ℓ, and mesons m to be

$$\mathcal{E} = \sum_{j=B,\ell,m}\mathcal{E}_j = \sum_{i=B,\ell}\frac{(2J_i+1)}{(2\pi)^3}\int\theta(k_{F_i} - |\vec{k}|)$$
$$\times\sqrt{k^2 + (M_i^*)^2}\,d^3k + \sum_{\alpha=\sigma,\omega,\rho}\frac{1}{2}m_\alpha^2\langle\alpha\rangle^2, \tag{16}$$

$$P = \sum_{j=B,\ell,m}P_j = \sum_{i=B,\ell}\frac{(2J_i+1)}{3(2\pi)^3}\int\frac{k^2\,\theta(k_{F_i} - |\vec{k}|)}{\sqrt{k^2 + (M_i^*)^2}}\,d^3k$$
$$+ \sum_{\alpha=\omega,\rho}\frac{1}{2}m_\alpha^2\langle\alpha\rangle^2 - \frac{1}{2}m_\sigma^2\langle\sigma\rangle^2, \tag{17}$$

where J_i is the spin of particle i ($J_i = \frac{1}{2}\forall i \in \{B,\ell\}$), which in this case accounts for the availability of both up and down spin states. $\theta(x)$ is the Heaviside step function. Note that the pressure arising from the vector mesons is positive, while it is negative for the scalar meson.

TABLE II. Couplings for QHD with the octet of baryons, fit to saturation of nuclear matter.

$g_{\sigma N}$	$g_{\omega N}$	g_ρ
10.644	13.179	6.976

The total baryon density ρ can be calculated via

$$\rho = \sum_B \rho_B = \sum_B \frac{(2J_B + 1)}{(2\pi)^3}\int\theta(k_{F_B} - |\vec{k}|)d^3k, \tag{18}$$

where in symmetric matter, the Fermi momenta are related via $k_F = k_{F_n} = k_{F_p}$, and the binding energy per baryon E is determined via

$$E = \left[\frac{1}{\rho}\left(\mathcal{E} - \sum_B M_B\rho_B\right)\right]. \tag{19}$$

The couplings $g_{\sigma N}$ and $g_{\omega N}$ are determined such that symmetric nuclear matter (in which $\rho_p = \rho_n = 0.5\rho$) saturates with the appropriate minimum in the binding energy per baryon of $E_0 = -15.86$ MeV at a nuclear density of $\rho_0 = 0.16$ fm^{-3}. The couplings for QHD that provide a fit to saturated nuclear matter are shown in Table II.

The coupling g_ρ is fixed such that the nucleon symmetry energy, given by

$$a_{\text{sym}} = \frac{g_\rho^2}{12\pi^2 m_\rho^2}k_F^3 + \frac{1}{12}\frac{k_F^2}{\sqrt{k_F^2 + (M_p^*)^2}} + \frac{1}{12}\frac{k_F^2}{\sqrt{k_F^2 + (M_n^*)^2}}, \tag{20}$$

is reproduced at saturation as $(a_{\text{sym}})_0 = 32.5$ MeV.

The chemical potential for any particle, μ_i, can be related to two independent chemical potentials—we choose that of the neutron (μ_n) and the electron (μ_e)—and thus we use a general relation

$$\mu_i = B_i\mu_n - Q_i\mu_e;$$
$$i \in \{p, n, \Lambda, \Sigma^+, \Sigma^0, \Sigma^-, \Xi^0, \Xi^-, \ell\}, \tag{21}$$

where B_i and Q_i are the baryon (unitless) and electric (in units of the proton charge) charges, respectively. For example, the proton has $B_p = +1$ and $Q_p = +1$, so it must satisfy $\mu_p = \mu_n - \mu_e$, which is familiar as β equilibrium. Since neutrinos are able to escape the star, we consider $\mu_\nu = 0$. Leptons have $B_\ell = 0$, and all baryons have $B_B = +1$.

The relations between the chemical potentials are therefore derived to be

$$\mu_\Lambda = \mu_{\Sigma^0} = \mu_{\Xi^0} = \mu_n,$$
$$\mu_{\Sigma^-} = \mu_{\Xi^-} = \mu_n + \mu_e,$$
$$\mu_p = \mu_{\Sigma^+} = \mu_n - \mu_e, \tag{22}$$
$$\mu_\mu = \mu_e.$$

The EOS for QHD can be obtained by finding solutions to Eqs. (7)–(9) subject to charge neutrality, conservation of a chosen total baryon number, and equivalence of chemical

potentials. These conditions can be summarized as

$$\left.\begin{array}{l} 0 = \sum_i Q_i \rho_i, \\ \rho = \sum_i B_i \rho_i, \\ \mu_i = B_i \mu_n - Q_i \mu_e, \end{array}\right\} \tag{23}$$

$$i \in \{p, n, \Lambda, \Sigma^+, \Sigma^0, \Sigma^-, \Xi^0, \Xi^-, \ell\}.$$

With these conditions, we are able to find the EOS for QHD. It should be noted that, as with many relativistic models for baryonic matter, once we include more than one species of baryon this model eventually produces baryons with negative effective masses at sufficiently high densities ($\rho > 1$ fm^{-3}). This is a direct result of the linear nature of the effective mass as shown in Eq. (11). As the Fermi energy [see Eq. (12)] approaches zero, the cost associated with producing baryon-antibaryon pairs is reduced, and at this point the model breaks down. From a more physical point of view, as the density rises, one would expect that the internal structure of the baryons should play a role in the dynamics. Indeed, within the QMC model, the response of the internal structure of the baryons to the applied mean scalar field ensures that no baryon mass ever becomes negative. We now describe the essential changes associated with the QMC model.

III. QMC MODEL

Like QHD, QMC is a relativistic quantum field theory formulated in terms of the exchange of scalar and vector mesons. However, in contrast with QHD these mesons couple not to structureless baryons but to clusters of confined quarks. As the density of the medium grows and the mean scalar and vector fields grow, the structure of the clusters adjusts self-consistently in response to the mean-field coupling. While such a model would be extremely complicated to solve in general, it has been shown by Guichon *et al.* [27] that in finite nuclei one should expect the Born-Oppenheimer approximation to be good at the 3% level. Of course, in nuclear matter it is exact at mean-field level.

Within the Born-Oppenheimer approximation, the major effect of including the structure of the baryon is that the internal quark wave functions respond in a way that opposes the applied scalar field. To a very good approximation, this physics is described through the "scalar polarizability," d, which in analogy with the electric polarizability describes the term in the baryon effective mass quadratic in the applied scalar field [21,28–31]. Recent explicit calculations of the equivalent energy functional for the QMC model have demonstrated the very natural link between the existence of the scalar polarizability and the many-body forces, or equivalently the density dependence, associated with successful, phenomenological forces of the Skyrme type [14,15]. In nuclear matter, the scalar polarizability is the *only* effect of the internal structure in mean-field approximation. On the other hand, in finite nuclei, the variation of the vector field across the hadronic volume also leads to a spin-orbit term in the nucleon energy [27].

Once one chooses a quark model for the baryons and specifies the quark-level meson couplings, there are no new parameters associated with introducing any species of

baryon into the nuclear matter. Given the well-known lack of experimental constraints on the forces between nucleons and hyperons, let alone hyperons and hyperons, which will be of great practical importance as the nuclear density rises above $(2–3)\rho_0$, this is a particularly attractive feature of the QMC approach, and it is crucial to our current investigation. Indeed, we point to the very exciting recent results of the QMC model, modified to include the effect of the scalar field on the hyperfine interaction, which led to Λ hypernuclei being bound in quite good agreement with experiment and Σ hypernuclei being unbound because of the modification of the hyperfine interaction [17], thus yielding a very natural explanation of this observed fact. We note the success that this description has found for finite nuclei, as noted in Ref. [15].

While we focus on the MIT bag model [32] as our approximation to baryon structure, we note that there has been a parallel development [33] based upon the covariant, chiral symmetric Nambu-Jona-Lasinio (NJL) model [34], with quark confinement modeled using the proper time regularization proposed by the Tübingen group [35,36]. The latter model has many advantages for the computation of the medium modification of form factors and structure functions, with the results for spin structure functions [37,38] offering a unique opportunity to experimentally test the fundamental idea of the QMC model. However, in both models, it is the effect of quark confinement that leads to a positive polarizability and a natural saturation mechanism.

Although the underlying physics of QHD and QMC is rather different, the equations to be solved are very similar at the hadronic level. We therefore focus on the changes that are required.

1. Because of the scalar polarizability of the hadrons, which accounts for the self-consistent response of the internal quark structure of the baryon to the applied scalar field [15], the effective masses appearing in QMC are nonlinear in the mean σ field. We write them in the general form

$$M_B^* = M_B - w_B^\sigma \, g_{\sigma N} \langle \sigma \rangle + \frac{d}{2} \tilde{w}_B^\sigma \, (g_{\sigma N} \langle \sigma \rangle)^2, \tag{24}$$

where the weightings w_B^σ and $\tilde{w}_B^\sigma$ and the scalar polarizability of the nucleon, d, must be calculated from the underlying quark model. Note now that only the coupling to the nucleons, $g_{\sigma N}$, is required to determine all the effective masses.

The most recent calculation of these effective masses, including the in-medium dependence of the spin-dependent hyperfine interaction [17], yields the explicit expressions:

$$M_N(\langle \sigma \rangle) = M_N - g_{\sigma N} \langle \sigma \rangle + \big[0.0022 + 0.1055 R_N^{\text{free}}$$
$$- 0.0178 \big(R_N^{\text{free}}\big)^2\big] (g_{\sigma N} \langle \sigma \rangle)^2,$$

$$M_\Lambda(\langle \sigma \rangle) = M_\Lambda - \big[0.6672 + 0.0462 R_N^{\text{free}}$$
$$- 0.0021 \big(R_N^{\text{free}}\big)^2\big] g_{\sigma N} \langle \sigma \rangle + \big[0.0016$$
$$+ 0.0686 R_N^{\text{free}} - 0.0084 \big(R_N^{\text{free}}\big)^2\big] (g_{\sigma N} \langle \sigma \rangle)^2,$$

$$M_\Sigma(\langle \sigma \rangle) = M_\Sigma - \big[0.6706 - 0.0638 R_N^{\text{free}}$$
$$- 0.008 \big(R_N^{\text{free}}\big)^2\big] g_{\sigma N} \langle \sigma \rangle + \big[-0.0007$$
$$+ 0.0786 R_N^{\text{free}} - 0.0181 \big(R_N^{\text{free}}\big)^2\big] (g_{\sigma N} \langle \sigma \rangle)^2,$$
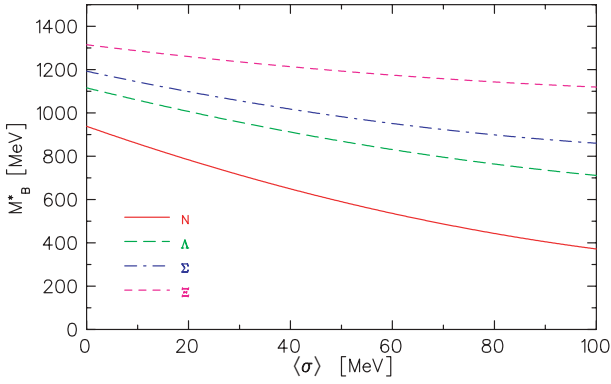
FIG. 1. (Color online) Baryon effective masses within the QMC model, parametrized as a function of the mean scalar field $\langle\sigma\rangle$. The values at $\langle\sigma\rangle = 0$ are the vacuum masses found in Table I. We show the effective masses only up to $\langle\sigma\rangle = 100$ MeV, which corresponds to about 2 fm^{-3} [(6–8)ρ_0], beyond which higher order terms not shown in Eq. (24) become significant.

$$M_\Xi(\langle\sigma\rangle) = M_\Xi - \left[0.3395 + 0.02822R_N^{\text{free}} \right.$$
$$\left. - 0.0128\left(R_N^{\text{free}}\right)^2\right]g_{\sigma N}\langle\sigma\rangle + \left[-0.0014\right.$$
$$\left. + 0.0416R_N^{\text{free}} - 0.0061\left(R_N^{\text{free}}\right)^2\right]\left(g_{\sigma N}\langle\sigma\rangle\right)^2. \tag{25}$$

We take $R_N^{\text{free}} = 0.8$ fm as the preferred value of the free nucleon radius, although in practice the numerical results depend only very weakly on this parameter [15].

Given the parameters in Eq. (25), all the effective masses for the baryon octet are entirely determined. They are plotted as functions of $\langle\sigma\rangle$ in Fig. 1, and we see clearly that they never become negative. [Note that the range of $\langle\sigma\rangle$ covered here corresponds to densities up to (6–8)ρ_0].

2. Since the mean scalar field $\langle\sigma\rangle$ is derived self-consistently by taking the derivative of the energy density with respect to $\langle\sigma\rangle$, the scalar field equation

$$\langle\sigma\rangle = \sum_B \frac{g_{\sigma N}}{m_\sigma^2} C(\langle\sigma\rangle) \frac{(2J_B + 1)}{(2\pi)^3} \int \frac{M_B^* \, \theta(k_{F_B} - |\vec{k}|)}{\sqrt{k^2 + (M_B^*)^2}} \, d^3k, \tag{26}$$

has an extra factor, denoted by

$$C(\langle\sigma\rangle) = \left[w_B^\sigma - \tilde{w}_B^\sigma dg_{\sigma N}\langle\sigma\rangle\right]. \tag{27}$$

Note that the d term (the scalar polarizability) in $C(\langle\sigma\rangle)$ does not have the factor of $\frac{1}{2}$ that is found Eq. (24), because of the differentiation.

Given this new term in the equation for the mean scalar field, we can see that this allows feedback of the scalar field which is modeling the internal degrees of freedom of the baryons. This feedback prevents certain values of $\langle\sigma\rangle$ from being accessed.

3. The couplings to the proton are redetermined by the fit to saturation properties (minimum binding energy per baryon and saturation density) with the new effective masses for the proton and neutron. The couplings for QMC that provide a fit to saturated nuclear matter are shown in Table III.

Given these changes alone, QHD is transformed into QMC. When we compare the results of Sec. VII with those of

TABLE III. Couplings for QMC with the octet of baryons, fit to saturation of nuclear matter.

$g_{\sigma N}$	$g_{\omega N}$	g_ρ
8.278	8.417	8.333

Ref. [16], minor differences arise because the QMC calculations in Ref. [16] are performed at the Hartree-Fock level, whereas here they have been performed at the Hartree level (mean-field) only.

IV. DECONFINED QUARK MATTER

We consider two models for a deconfined quark matter phase, both of which model free quarks in β equilibrium. The first model, the MIT bag model [32], is commonly used to describe the quark matter phase because of its simplicity.

In this model, we consider three quarks with fixed masses to possess chemical potentials related to the independent chemical potentials of Eq. (21) via

$$\mu_u = \tfrac{1}{3}\mu_n - \tfrac{2}{3}\mu_e, \quad \mu_d = \tfrac{1}{3}\mu_n + \tfrac{1}{3}\mu_e, \quad \mu_s = \mu_d, \tag{28}$$

where quarks have a baryon charge of $\frac{1}{3}$ since baryons contain three quarks. Because the quarks are taken to be free, the chemical potential has no vector interaction terms, and thus

$$\mu_q = \sqrt{k_{F_q}^2 + m_q^2}; \quad q \in \{u, d, s\}. \tag{29}$$

The EOS can therefore be solved under the conditions of Eq. (23).

As an alternative model for deconfined quark matter, we consider a simplified NJL model [34], in which the quarks have dynamically generated masses, ranging from constituent quark masses at low densities to current quark masses at high densities. The equation for a quark condensate at a given density (and hence, k_F) in NJL is similar to the scalar field in QHD/QMC and is written as

$$\langle\bar{\psi}\psi\rangle = -4\mathcal{N}_c \int \frac{1}{(2\pi^3)} \frac{M_q^* \, \theta(k_F - |\vec{k}|) \, \theta(\Lambda - k_F)}{\sqrt{k^2 + (M_q^*)^2}} \, d^3k, \tag{30}$$

where M_q^* denotes the k_F-dependent (hence, density-dependent) quark mass; $\mathcal{N}_c$ is the number of color degrees of freedom of quarks; and Λ is the momentum cutoff. This is self-consistently calculated via

$$M_q^* = M_{\text{current}} - G\langle\bar{\psi}\psi\rangle, \tag{31}$$

where G is the coupling and M_{current} the current quark mass.

To solve for the quark mass at each density, we must first find the coupling G that yields the required constituent quark mass in free space ($k_F = 0$). The coupling is assumed to remain constant as the density rises. In free space, we can solve the
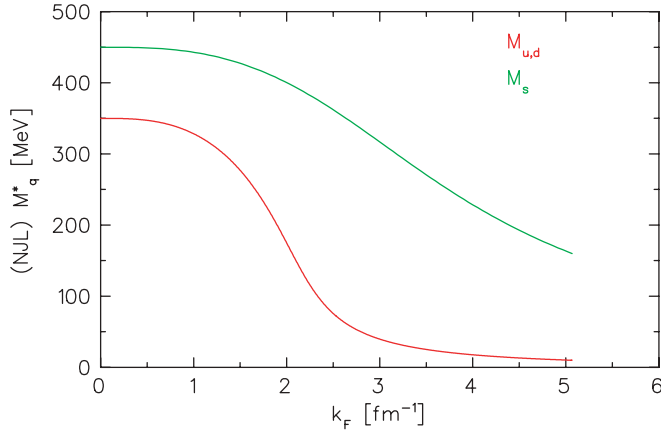
FIG. 2. (Color online) Density-dependent (dynamic) masses for quarks using NJL. The mass at $k_F = 0$ is the constituent quark mass, and the mass at the cutoff of $k_F = \Lambda$ is roughly the current quark mass. This model successfully reproduces the behavior found within the Schwinger-Dyson formalism, and we consider the model to be more sophisticated than the constant quark mass MIT bag model.

above equations to find the coupling:

$$
G = \frac{(M_q^* - M_{\text{current}})}{4\mathcal{N}_c} \left[\int \frac{1}{(2\pi)^3} \right.
$$

$$
\left. \times \frac{M_q^* \, \theta(|\vec{k}| - k_F) \, \theta(\Lambda - k_F)}{\sqrt{k^2 + (M_q^*)^2}} \, d^3k \right]^{-1} \Bigg|_{k_F=0}. \quad (32)
$$

We solve Eqs. (30)–(32) for $\mathcal{N}_c = 3$ to obtain constituent quark masses of $M_{u,d} = 350$ MeV using current quark masses of $M_{\text{current}} = 10$ MeV for the light quarks, and to obtain a constituent quark mass of $M_s = 450$ MeV using a current quark mass of $M_{\text{current}} = 160$ MeV for the strange quark, with a momentum cutoff of $\Lambda = 1$ GeV. At $k_F = 0$, we find the couplings to be

$$
G_{u,d} = 0.148 \, \text{fm}^2, \quad G_s = 0.105 \, \text{fm}^2. \quad (33)
$$

We can now use these parameters to evaluate the dynamic quark mass M_q^*, for varying values of k_F, by solving Eqs. (30) and (31) self-consistently. The resulting density dependence of M_q^* is illustrated in Fig. 2. This shows that the quark masses eventually saturate and are somewhat constant above a certain density. We can then construct the EOS in the same way as we did for the MIT bag model, but with density-dependent masses rather than fixed masses.

V. PHASE TRANSITIONS

A. Equilibrium conditions

We now have a description of hadronic matter with quark degrees of freedom, but we are still faced with the issue that the baryons are very densely packed. We wish to know if it is more energetically favorable for deconfined quark matter to be the dominant phase at a certain density. To do this, we need to

find a point (if it exists) at which stability is achieved between the hadronic phase and the quark phase.

The condition for stability is that chemical, thermal, and mechanical equilibrium between the hadronic (H) and quark (Q) phases is achieved, and thus that the independent quantities in each phase are separately equal. Thus the two independent chemical potentials (μ_n, μ_e) are each separately equal to their counterparts in the other phase, i.e., $(\mu_n)_H = (\mu_n)_Q$, and $(\mu_e)_H = (\mu_e)_Q$ (chemical equilibrium); the temperatures are equal ($T_H = T_Q$) (thermal equilibrium); and the pressures are equal ($P_H = P_Q$) (mechanical equilibrium). For a discussion of this condition, see Ref. [39]. We consider both phases to be cold on the nuclear scale, and assume $T = 0$, so the temperatures are by construction equal. We must therefore find the point at which, for a given pair of independent chemical potentials, the pressures in both the hadronic phase and the quark phase are the same.

To find the partial pressure of any baryon, quark, or lepton species, i, we use

$$
P_i = \frac{(2J_B + 1)\mathcal{N}_c}{3(2\pi)^3} \int \frac{k^2 \, \theta\left(k_{F_i} - |\vec{k}|\right)}{\sqrt{k^2 + (M_i^*)^2}} \, d^3k, \quad (34)
$$

where $\mathcal{N}_c = 3$ for quarks, and $\mathcal{N}_c = 1$ for baryons and leptons. To find the total pressure in each phase, we use

$$
P_H = \sum_B P_B + \sum_\ell P_\ell + \sum_{\alpha=\omega,\rho} \frac{1}{2} m_\alpha^2 \langle \alpha \rangle^2 - \frac{1}{2} m_\sigma^2 \langle \sigma \rangle^2, \quad (35)
$$

which is equivalent to Eq. (17), and

$$
P_Q = \sum_q P_q + \sum_\ell P_\ell - B, \quad (36)
$$

where B in the quark pressure is the bag energy density. For the QMC model described in Sec. III, and a Fermi gas of quarks, both with interactions with leptons for charge neutrality, a point exists at which the condition of stability, as described above, is satisfied.

At this point, it is equally favorable that hadronic matter and quark matter are the dominant phase. Beyond this point, the quark pressure is greater than the hadronic pressure, and so the quark phase has a lower thermodynamic potential (through the relation $P = -\Omega$) and the quark phase will be more energetically favorable. To determine the EOS beyond this point, we need to consider a mixed phase.

B. Mixed phase

We can model a mixed phase of hadronic and quark matter—as opposed to modeling a simple direct phase transition between the two, a Maxwell construction, which would have a discontinuity in the density while retaining a constant pressure between the two phases—using the method of Glendenning. A detailed description of this appears in Ref. [18].

We solve for the hadronic EOS using the independent chemical potentials as inputs for the quark matter EOS with increasing order parameter ρ (the conserved baryon density) until we find a point (if it exists) at which the pressure in the
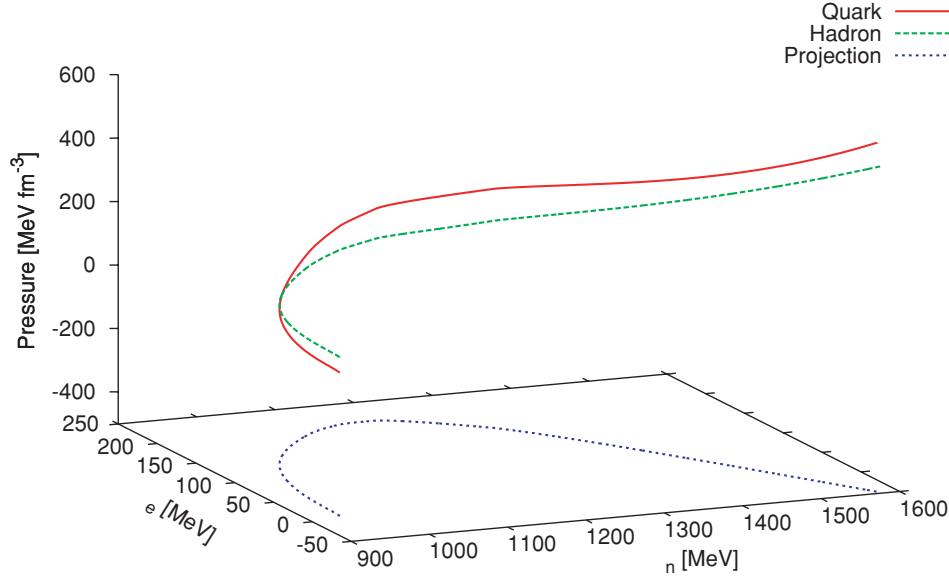
FIG. 3. (Color online) Illustrative locus of values for μ_e, μ_n, P for phases of hadronic matter and deconfined quark matter. Note that pressure increases with density, and a projection onto the $\mu_n \mu_e$ plane is a single line, as ensured by the chemical equilibrium condition.

quark phase is equal to that in the hadronic phase. Once we have the density and pressure at which the phase transition occurs, we change the order parameter from the conserved baryon density to the quark fraction χ. If we consider the mixed phase to be a fraction of the hadronic matter and a fraction of the quark matter, then the mixed phase (MP) of matter will have the following properties: the total density will be

$$\rho_{\mathrm{MP}} = (1 - \chi)\, \rho_{\mathrm{HP}} + \chi\, \rho_{\mathrm{QP}}, \qquad (37)$$

where ρ_{HP} and ρ_{QP} are the densities in the hadronic and quark phases, respectively. The equivalent baryon density in the quark phase,

$$\rho_{\mathrm{QP}} = \sum_q \rho_q = 3(\rho_u + \rho_d + \rho_s), \qquad (38)$$

arises because of the restriction that a bag must contain three quarks.

According to the condition of mechanical equilibrium, the pressure in the mixed phase will be

$$P_{\mathrm{MP}} = P_{\mathrm{HP}} = P_{\mathrm{QP}}. \qquad (39)$$

We can step through values $0 < \chi < 1$ and find the density at which equilibrium is achieved, keeping the mechanical stability conditions as they were above. In the mixed phase, we need to alter our definition of charge neutrality; it becomes possible now that one phase is (locally) charged, while the other phase carries the opposite charge, making the system globally charge neutral. This is achieved by enforcing

$$0 = (1 - \chi)\, \rho^c_{\mathrm{HP}} + \chi\, \rho^c_{\mathrm{QP}} + \rho^c_\ell, \qquad (40)$$

where this time we are considering charge densities, which are simply charge proportions of density, and ρ^c_ℓ is the lepton charge density. For example, the charge density in the quark phase is given by

$$\rho^c_{\mathrm{QP}} = \sum_q Q_q \rho_q = \frac{2}{3}\rho_u - \frac{1}{3}\rho_d - \frac{1}{3}\rho_s. \qquad (41)$$

We continue to calculate the densities until we reach $\chi = 1$, at which point the mixed phase is now entirely charge-neutral quark matter. After this point, we continue with the EOS for pure charge-neutral quark matter, using ρ as the order parameter.

VI. STELLAR SOLUTIONS

To test the predictions of these models, we find solutions of the Tolman-Oppenheimer-Volkoff (TOV) [40] equation

$$\frac{dP}{dR} = -\frac{G\,(P + \mathcal{E})\,(M(R) + 4\pi R^3 P)}{R(R - 2GM(R))}, \qquad (42)$$

where the mass $M(R)$ contained within a radius R is found by integrating the energy density

$$M(R) = \int_0^R 4\pi r^2 \mathcal{E}\, dr, \qquad (43)$$

and $\mathcal{E}$ and P are the energy density and pressure in the EOS, respectively.

Given an EOS and a choice for the central density of the star, this provides static, spherically symmetric, nonrotating, gravitationally stable stellar solutions for the total mass and radius of a star. For studies of the effect of rapid rotation in general relativity, we refer to Refs. [41,42]. This becomes important for comparison with experimental data; as only data for stellar masses exist (with the single, disputed exception from Ref. [12]), we can use the model to predict the radii of the observed stars.

VII. RESULTS

To obtain numerical results, we solve the meson field equations (7)–(9), with the conditions of charge neutrality, fixed baryon density, and the equivalence of chemical potentials given by Eq. (23), for various models. Having found the EOS by evaluating the energy density, Eq. (16), and pressure,
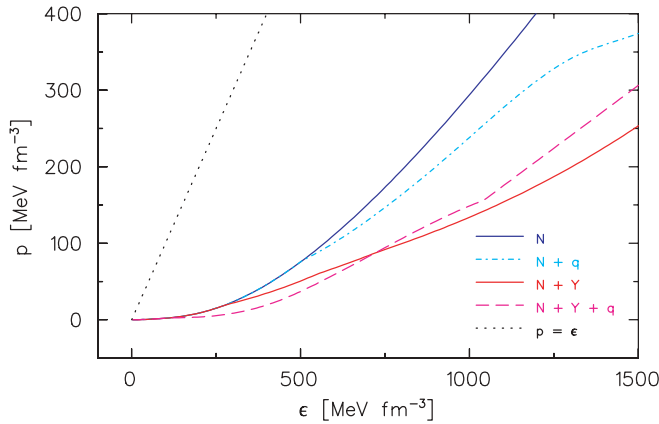
FIG. 4. (Color online) Equations of state for nucleonic 'N' matter modeled with octet QMC but where hyperons are explicitly forbidden; nucleonic matter where a phase transition to NJL modeled quark matter is permitted; baryonic 'N+Y' matter modeled with octet QMC including hyperons; and baryonic matter where a phase transition to MIT bag modeled quark matter is permitted. The line $P = \mathcal{E}$ represents the causal limit, $v_{\text{sound}} = c$. The bends in these curves indicate a change in the composition of the EOS, such as the creation of hyperons or a transition to a mixed or quark phase. Note that at low energies (densities) the curves are identical, where only nucleonic matter in β-equilibrium is present.

Eq. (17), we can solve for stellar solutions for an EOS using the TOV equation. The radius of the star is defined as the radius at which the pressure is zero and is calculated using a fourth-order Runge-Kutta integration method.

The EOS for octet QMC hadronic matter is shown in Fig. 4 alongside the same model when including a phase transition to three-flavor quark matter modeled with the MIT bag model, and the results do not appear to differ much at this scale. The theoretical causality limit of $P = \mathcal{E}$ is also shown (corresponding to the limit $v_{\text{sound}} = c$), and we can see that these models do not approach this limit at the scale displayed. This is because of the softening of the EOS that occurs with the introduction of hyperons, enlarging the Fermi sea to be filled and reducing the overall pressure.

The species fraction for each particle, Y_i, is simply the density fraction of that particle and is calculated via

$$Y_i = \frac{\rho_i}{\rho}, \quad i \in \{p, n, \Lambda, \Sigma^+, \Sigma^0, \Sigma^-, \Xi^0, \Xi^-, \ell, q\}, \quad (44)$$

where ρ is the total baryon density. The species fractions for octet QMC when a phase transition is neglected are shown in Fig. 5, where we note that the Λ species fraction is enhanced and the Σ species fractions are suppressed with increasing density. From the investigations by Rikovska-Stone et al. [16], we expect that the Σ would disappear entirely if we were to include Fock terms.

The values of the compression modulus and effective nucleon mass at saturation are frequently used as a comparison with experimental evidence. Models that neglect quark-level interactions, such as QHD, typically predict much higher values for the compression modulus than experiments suggest. In the symmetric (nuclear) matter QHD model described in this paper, we find values of $(M^*/M)_{\text{sat}} = 0.56$ and $K =$
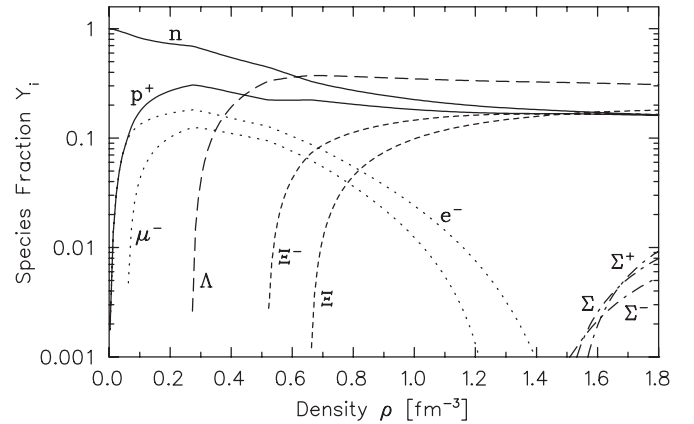

FIG. 5. Species fractions Y_i for octet QMC where a transition to a mixed phase is explicitly forbidden. Note that in this case, all of the octet baryons contribute at some density, and with increasing density the species fractions of Σ hyperons are suppressed, while the Λ species fraction is enhanced. Parameters used here are shown in Table III.

525 MeV, which are in agreement with those stated in Ref. [19], but as noted by those authors, not with experiment. For QMC, we find a significant improvement in the compression modulus, $K = 280$ MeV which lies at the upper end of the experimental range. The nucleon effective mass at saturation for QMC is found to be $(M^*)_{\text{sat}} = 735$ MeV, producing $(M^*/M)_{\text{sat}} = 0.78$.

When we calculate the EOS including a mixed phase and subsequent pure quark phase, we find that small changes in the parameters can sometimes lead to very significant changes. In particular, the bag energy density B and the quark masses in the MIT bag model have the ability to both move the phase transition points and vary the constituents of the mixed phase. We have investigated the range of parameters that yield a transition to a mixed phase, and these are summarized in Table IV. For illustrative purposes, we show an example of species fractions for a reasonable set of parameters ($B^{1/4} = 180$ MeV and $m_{u,d,s} = 3, 7, 95$ MeV) in Fig. 6. Note that in this case the Λ hyperon enters the mixed phase briefly (and at a low species fraction).

Note that the transition density of $\rho_{\text{MP}} \sim 0.12$ fm^{-3} produced by the combination of the octet QMC and MIT bag models (as shown in Fig. 6) is clearly not physical, as it implies the presence of deconfined quarks at densities less than ρ_0.

With small changes to parameters, such as those used to produce Fig. 7 in which the bag energy density is given a slightly higher value from that used in Fig. 6 ($B^{1/4}$ increases from 180 to 195 MeV, but the quark masses remain the same), it becomes possible for the Ξ hyperons to also enter the mixed phase, albeit in that case with small species fractions, $Y_\Sigma, Y_\Xi \leqslant 0.02$.

The TOV solutions for octet QMC with and without a phase transition to a mixed phase are shown in Fig. 8. The stellar masses produced using these methods are similar to observed neutron star masses. Once we have solved the TOV equations, we can examine individual solutions and determine the species content for specific stars. If we examine the solutions with a

TABLE IV. Species content (N = nucleons, Y = hyperons, ℓ = leptons, q = quarks), inputs ($B^{1/4}$, m_q), and results for octet QMC and quark models presented in this paper. ρ_Y, ρ_{MP}, and ρ_{QP} represent, respectively, the density at which hyperons first appear (Λ is invariably the first to enter in these calculations), the density at which the mixed phase begins, and the density at which the quark phase begins. Figures for selected parameter sets are referenced in the final column. Dynamic NJL quark masses are determined by Eqs. (30)–(32).

Particles	$B^{1/4}$ (MeV)	$\{m_u, m_d, m_s\}$ (MeV)	ρ_Y (fm^{-3})	ρ_{MP} (fm^{-3})	ρ_{QP} (fm^{-3})	Fig.
N, Y, ℓ	–	–	0.27	–	–	5
N, Y, ℓ, q	180	$\{3, 7, 95\}$	0.55	0.12	0.95	6
N, Y, ℓ, q	195	$\{3, 7, 95\}$	0.35	0.24	1.46	7
N, Y, ℓ, q	170	$\{30, 70, 150\}$	0.56	0.10	0.87	–
N, Y, ℓ, q	175	$\{100, 100, 150\}$	0.44	0.16	1.41	–
N, ℓ, q	180	Dynamic (NJL)	–	0.47	1.67	13

stellar mass of $M = 1.2M_\odot$, where $M_\odot$ is the solar mass, for the set of parameters used to produce Figs. 5 and 6, we can find the species fraction as a function of stellar radius to obtain a cross section of the star. This is shown in Fig. 9 for the case of no phase transition and in Fig. 10 for the case where we allow a transition to a mixed phase and subsequently to a quark matter phase.

If we now examine the stellar solution with mass $M = 1.2M_\odot$ of the set of parameters ($B^{1/4} = 195$ MeV and $m_{u,d,s} = 3, 7, 95$ MeV used to produce Fig. 7) as shown in Fig. 11, we note that the quark content of this 10.5 km star reaches out to around 8 km, and that the core of the star contains roughly equal proportions of protons, neutrons, and Λ hyperons, with $Y_i \simeq 10\%$.

Within a mixed phase, we require that for a given pair of μ_n and μ_e at any value of the mixing parameter χ, the quark density is greater than the hadronic density. This condition ensures that the total baryon density increases monotonically

within the range $\rho_{QP} > \rho_{MP} > \rho_{HP}$, as can be seen in Eq. (37). An example of this is illustrated in Fig. 12 for a mixed phase of octet QMC and three-flavor quark matter modeled with the MIT bag model.

The use of quark masses corresponding to the NJL model results in a quark density that is lower than the hadronic density, and as a result there are no solutions for a mixed phase in which the proportion of quarks increases with fraction χ, while at the same time the total baryon density increases. It may be possible that with smaller constituent quark masses at low density, the Fermi momenta would provide sufficiently high quark densities, but we feel that it would be unphysical to use any smaller constituent quark masses. This result implies that, at least for the model we have investigated, dynamical chiral symmetry breaking (in the production of constituent quark masses at low density) prevents a phase transition from a hadronic phase to a mixed phase involving quarks.

We do note, however, that if we restrict consideration to nucleons only within the QMC model (with the same parameters as octet QMC) and represent quark matter with the NJL model, we do in fact find a possible mixed phase. More surprisingly, the phase transition density for this combination

FIG. 6. Same as Fig. 5, but now we allow the phase transition to a mixed phase involving quark matter modeled with the MIT bag model, and subsequently to a pure deconfined quark matter phase. Parameters used here are summarized in Table IV. Note that with these parameters, the Λ is the only hyperon to appear in the mixed phase, and it does so at a much higher density than when the transition to a mixed phase is forbidden. We also note that with these parameters, the transition to a mixed phase occurs below the saturation density ρ_0.

FIG. 7. Same as Fig. 6, but now the bag energy density has been increased to $B^{1/4} = 195$ MeV. Note that now the appearance of hyperons occurs at a smaller density than in Fig. 6, the transition to a mixed phase occurs at a slightly larger density, and Ξ hyperons are present in the mixed phase.
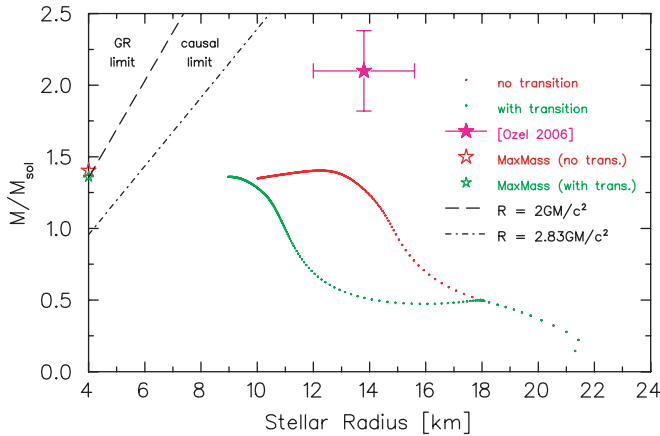
FIG. 8. (Color online) Solutions of the TOV equations for the total stellar mass and radius for octet QMC, where a phase transition to mixed phase is explicitly forbidden (as shown in Fig. 5) and the same model with an allowed phase transition to three-flavor quark matter modeled with the MIT bag model (as in Fig. 6). Also shown is the data point from Ref. [12]. The points on the vertical axis are the maximum masses in the respective models. The causal and general relativistic limits on mass and radius are also shown.

FIG. 10. Species fractions for octet QMC with a phase transition to three-flavor quark matter modeled with the MIT bag model, as a function of stellar radius for a stellar solution with a total mass of $1.2 M_\odot$. The parameters used here are the same as those used to produce Fig. 6. Note that in this case, one finds pure deconfined three-flavor quark matter at the core (all of some 3.5 km) of this star, and still a small proportion of Λ in the mixed phase.

is significantly larger than the case where hyperons are present. An example of this is shown in Fig. 13 with parameters found in Table IV. This produces a mixed phase at about $3\rho_0(\rho = 0.47 \text{ fm}^{-3})$ and a pure quark matter phase above about $10.5\rho_0(\rho = 1.67 \text{ fm}^{-3})$. We note the coincidence of this phase transition density with the density corresponding to one nucleon per nucleon volume, with the aforementioned assumption of $R_N^{\text{free}} = 0.8$ fm, though we do not draw any conclusions from this. Performing this calculation with quark matter modeled with the MIT bag model produces results similar to those of Fig. 6, except of course lacking the Λ hyperon contribution. Although this example does show a phase transition, the omission of hyperons is certainly

unrealistic. This does, however, illustrate the importance and significance of including hyperons, in that their inclusion alters the chemical potentials that satisfy the equilibrium conditions in such a way that the mixed phase is no longer produced.

For each of the cases where we find a phase transition from baryonic matter to quark matter, the solution consists of negatively charged quark matter, positively charged hadronic matter, and a small proportion of leptons, to produce globally charge-neutral matter. The proportions of hadronic, leptonic, and quark matter throughout the mixed phase (for example, during a transition from octet QMC matter to three-flavor quark matter modeled with the MIT bag model) are displayed in
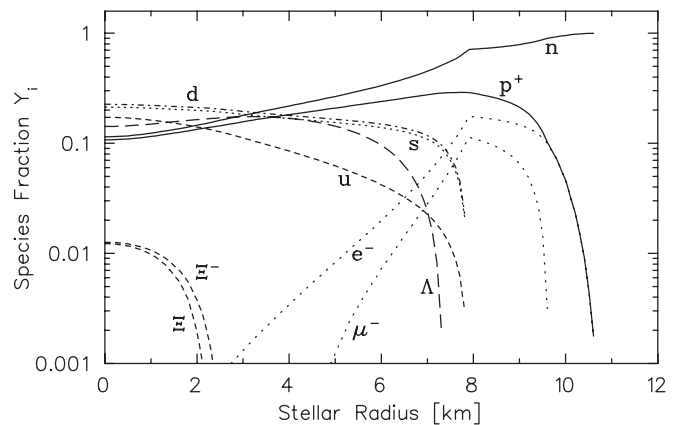

FIG. 9. Species fractions for octet QMC in β equilibrium, where the phase transition to a mixed phase is explicitly forbidden, as a function of stellar radius for a stellar solution with a total mass of $1.2 M_\odot$. The parameters used here are the same as those used to produce Fig. 5.

FIG. 11. Example of the interior of a star of total stellar mass $M = 1.2 M_\odot$ where the bag energy density is given a slightly higher value than that used in Fig. 10 (increased from $B^{1/4} = 180$ to 195 MeV), but the quark masses remain the same. This illustrates that with relatively minor adjustments to the parameters, large changes can be introduced to the final solution. In this case, Ξ hyperons can provide a nonzero contribution to the composition of a star. Note that in this case, quark matter appears at 8 km, and at the core there exists a mixed phase containing nucleons, quarks, and Λ, Ξ^0, and Ξ^- hyperons.
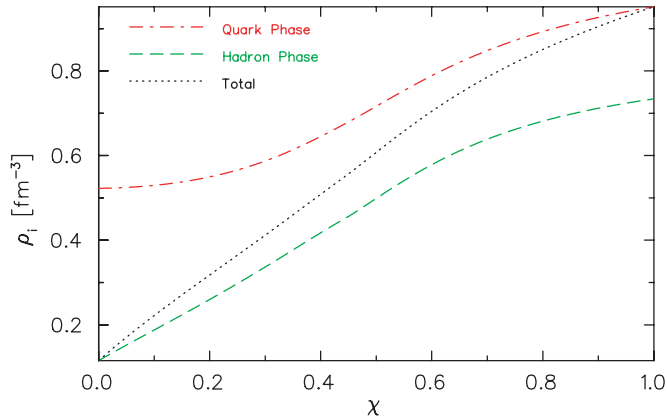
FIG. 12. (Color online) Densities in the mixed phase for octet QMC mixed with three-flavor quark matter modeled with the MIT bag model. Note that at all values of χ [the mixing parameter according to Eq. (37)], the equivalent quark baryon density is greater than the hadronic baryon density, allowing the total baryon density to increase monotonically. The total density is found via Eq. (37).
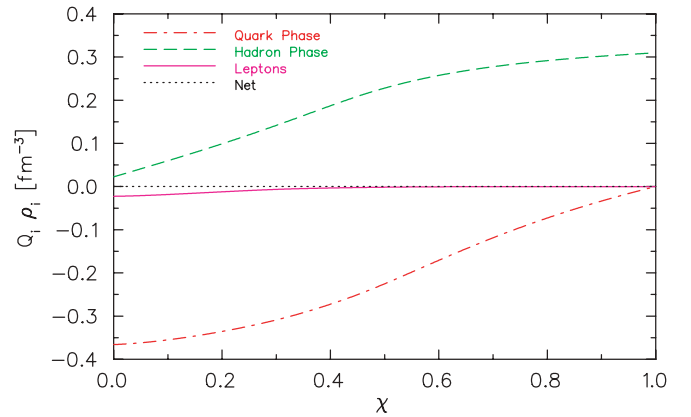

FIG. 14. (Color online) Charge densities (in units of the proton charge per cubic fm) in the mixed phase for a transition from octet QMC to three-flavor quark matter modeled with the MIT bag model. Note that following the mixed phase, the quarks are able to satisfy charge neutrality with no leptons. χ is the mixing parameter within the mixed phase according to Eq. (37).

Fig. 14. A summary of the results of interest is given in Table IV.

Results for larger quark masses are not shown, as they require a much lower bag energy density to satisfy the equilibrium conditions. For constituent quark masses, we find that no phase transition is possible for any value of the bag energy density, as the quark pressure does not rise sufficiently fast to overcome the hadronic pressure. This is merely because the mass of the quarks does not allow a sufficiently large Fermi momentum at a given chemical potential, according to Eq. (29).
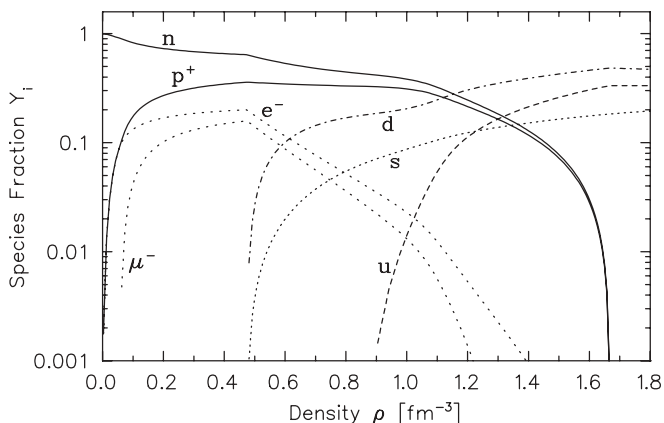

FIG. 13. Species fractions for a phase transition from QMC nuclear matter to three-flavor quark matter modeled with NJL. Note that in this unphysical case, a phase transition is possible and occurs at a value of about $\rho = 0.47$ fm^{-3}. We note the coincidence with the density of one baryon per baryon volume, but draw no conclusions from this. A similar transition from QMC nuclear matter to three-flavor quark matter modeled with the MIT bag model produces results almost identical to those of Fig. 6, except that in that case there is no contribution from the Λ hyperon.

VIII. CONCLUSIONS

We have produced several EOSs that simulate a phase transition from octet QMC modeled hadronic matter, via a continuous Glendenning style mixed phase, to a pure, deconfined quark matter phase. This should correspond to a reasonable description of the relevant degrees of freedom in each density region. The models used here for quark matter provide a framework for exploring the way that this form of matter may behave, in particular under extreme conditions. The success of the QMC model in reproducing a broad range of experimental data gives us considerable confidence in this aspect of these calculations and provides a reasonable hadronic sector and calculation framework, which then awaits improvement in the quark sector to produce realistic stellar solutions.

We have presented EOSs and stellar solutions for octet QMC matter at the Hartree level. We have explored several possible phase transitions from this hadronic sector to a mixed phase involving three-flavor quark matter. The corresponding EOSs demonstrate the complexity and intricacy of the solutions as well as the dependence on small changes in parameters. The stellar solutions provide overlap with the lower end of the experimentally acceptable range.

Several investigations were made of the response of the model to a more sophisticated treatment of the quark masses in-medium, namely, the NJL model. In that model the quark masses arise from dynamical chiral symmetry breaking and thus take values typical of constituent quarks at low density and drop to current quark masses at higher densities. The result is that no transition to a mixed phase is possible in this case.

The omission of hyperons in the QMC model yields a transition to a mixed phase of either NJL or MIT bag model quark matter, as the hadronic EOS is no longer as soft. This observation makes it clear that hyperons can play a significant role in the EOS. However, we acknowledge that their presence in neutron stars remains speculative.

The models considered here reveal some important things about the possible nature of the dense nuclear matter in a neutron star. It seems that if dynamical chiral symmetry does indeed result in typical constituent quark masses in low-density quark matter, then a phase transition from hadronic matter to quark matter is unlikely. This result invites further investigation.

The results presented in Fig. 8 indicate that the model in its current form is unable to reproduce sufficiently massive neutron stars to account for all observations, notably the observed stellar masses of $1.45 M_\odot$ and larger. This is a direct result of the softness of the EOS. This issue will be explored in a future publication via the inclusion of Fock terms, which have been shown to have an effect on the scalar and vector potentials [43].

Many open questions remain to be investigated in further work, including the effects of Fock terms, and the density dependence of the bag energy density in the quark phase, which can be calculated explicitly within the NJL model. The quark matter models used here are still not the most sophisticated models available, and future work may involve an investigation of the effects of color-superconducting quark matter [44,45].

ACKNOWLEDGMENTS

[1] P. Podsiadlowski *et al.*, Mon. Not. R. Astron. Soc. **361**, 1243 (2005).
[2] H. Grigorian, D. Blaschke, and T. Klahn, arXiv:astro-ph/0611595.
[3] T. Klahn *et al.*, Phys. Lett. **B654**, 170 (2007).
[4] J. M. Lattimer and M. Prakash, Astrophys. J. **550**, 426 (2001).
[5] H. Heiselberg and M. Hjorth-Jensen, Phys. Rep. **328**, 237 (2000).
[6] F. Weber, Prog. Part. Nucl. Phys. **54**, 193 (2005).
[7] J. Schaffner-Bielich, J. Phys. G **31**, S651 (2005).
[8] F. Weber and M. K. Weigel, Nucl. Phys. **A493**, 549 (1989).
[9] S. A. Chin and J. D. Walecka, Phys. Lett. **B52**, 24 (1974).
[10] P. Danielewicz, R. Lacey, and W. G. Lynch, Science **298**, 1592 (2002).
[11] A. Worley, P. G. Krastev, and B.-A. Li, Astrophys. J. (to be published), arXiv:0801.1653.
[12] F. Ozel, Nature (London) **441**, 1115 (2006).
[13] M. Alford *et al.*, Nature (London) **445**, E7 (2007).
[14] P. A. M. Guichon and A. W. Thomas, Phys. Rev. Lett. **93**, 132502 (2004).
[15] P. A. M. Guichon, H. H. Matevosyan, N. Sandulescu, and A. W. Thomas, Nucl. Phys. **A772**, 1 (2006).
[16] J. Rikovska-Stone, P. A. M. Guichon, H. H. Matevosyan, and A. W. Thomas, Nucl. Phys. **A792**, 341 (2007).
[17] P. A. M. Guichon, A. W. Thomas, and K. Tsushima, Nucl. Phys. **A814**, 66 (2008).
[18] N. K. Glendenning, Phys. Rep. **342**, 393 (2001).
[19] B. D. Serot and J. D. Walecka, Adv. Nucl. Phys. **16**, 1 (1986).
[20] R. J. Furnstahl and B. D. Serot, Comments Nucl. Part. Phys. **2**, A23 (2000).
[21] P. A. M. Guichon, Phys. Lett. **B200**, 235 (1988).
[22] K. Saito, K. Tsushima, and A. W. Thomas, Phys. Rev. C **55**, 2637 (1997).
[23] K. Saito, K. Tsushima, and A. W. Thomas, Prog. Part. Nucl. Phys. **58**, 1 (2007).

[24] H. Muller and B. K. Jennings, Nucl. Phys. **A626**, 966 (1997).
[25] W. M. Yao *et al.* (Particle Data Group), J. Phys. G **33**, 1 (2006).
[26] T. A. Rijken, V. G. J. Stoks, and Y. Yamamoto, Phys. Rev. C **59**, 21 (1999).
[27] P. A. M. Guichon, K. Saito, E. N. Rodionov, and A. W. Thomas, Nucl. Phys. **A601**, 349 (1996).
[28] A. W. Thomas, P. A. M. Guichon, D. B. Leinweber, and R. D. Young, Prog. Theor. Phys. Suppl. **156**, 124 (2004).
[29] M. Ericson and G. Chanfray, AIP Conf. Proc. **1030**, 13 (2008).
[30] E. Massot and G. Chanfray, Phys. Rev. C **78**, 015204 (2008).
[31] G. Chanfray, M. Ericson, and P. A. M. Guichon, Phys. Rev. C **68**, 035209 (2003).
[32] A. Chodos, R. L. Jaffe, K. Johnson, C. B. Thorn, and V. F. Weisskopf, Phys. Rev. D **9**, 3471 (1974).
[33] W. Bentz and A. W. Thomas, Nucl. Phys. **A696**, 138 (2001).
[34] Y. Nambu and G. Jona-Lasinio, Phys. Rev. **122**, 345 (1961).
[35] G. Hellstern, R. Alkofer, and H. Reinhardt, Nucl. Phys. **A625**, 697 (1997).
[36] D. Ebert, T. Feldmann, and H. Reinhardt, Phys. Lett. **B388**, 154 (1996).
[37] I. C. Cloet, W. Bentz, and A. W. Thomas, Phys. Rev. Lett. **95**, 052302 (2005).
[38] I. C. Cloet, W. Bentz, and A. W. Thomas, Phys. Lett. **B642**, 210 (2006).
[39] F. Reif, *Fundamentals of Statistical and Thermal Physics* (McGraw-Hill, New York, 1965).
[40] J. R. Oppenheimer and G. M. Volkoff, Phys. Rev. **55**, 374 (1939).
[41] J. M. Lattimer and B. F. Schutz, Astrophys. J. **629**, 979 (2005).
[42] B. J. Owen, Phys. Rev. Lett. **95**, 211101 (2005).
[43] G. Krein, A. W. Thomas, and K. Tsushima, Nucl. Phys. **A650**, 313 (1999).
[44] M. G. Alford, A. Schmitt, K. Rajagopal, and T. Schafer, Rev. Mod. Phys. **80**, 1455 (2008).
[45] S. Lawley, W. Bentz, and A. W. Thomas, J. Phys. G **32**, 667 (2006).